*Article*

# Influence of Laser Welding Speed on the Morphology and Phases Occurring in Spray-Compacted Hypereutectic Al-Si-Alloys

**Thomas Gietzelt [1],\*, Torsten Wunsch [1], Florian Messerschmidt [1], Holger Geßwein [2] and Uta Gerhards [1]**

[1] Karlsruhe Institute of Technology, Institute for Micro Process Engineering, P.O. Box 3640, 76021 Karlsruhe, Germany; torsten.wunsch@kit.edu (T.W.); florian.messerschmidt@kit.edu (F.M.); uta.gerhards@kit.edu (U.G.)

[2] Karlsruhe Institute of Technology, Institute for Applied Materials, P.O. Box 3640, 76021 Karlsruhe, Germany; holger.gesswein@kit.edu

\* Correspondence: thomas.gietzelt@kit.edu; Tel.: +49-721-608-23314

**Abstract:** Normally, the weldability of aluminum alloys is ruled by the temperature range of solidification of an alloy according to its composition by the formation of hot cracks due to thermal shrinkage. However, for materials at nonequilibrium conditions, advantage can be taken by multiple phase formation, leading to an annihilation of temperature stress at the microscopic scale, preventing hot cracks even for alloys with extreme melting range. In this paper, several spray-compacted hypereutectic aluminum alloys were laser welded. Besides different silicon contents, additional alloying elements like copper, iron and nickel were present in some alloys, affecting the microstructure. The microstructure was investigated at the delivery state of spray-compacted material as well as for a wide range of welding speeds ranging from 0.5 to 10 m/min, respectively. The impact of speed on phase composition and morphology was studied at different disequilibrium solidification conditions. At high welding velocity, a close-meshed network of eutectic Al-Si-composition was observed, whereas the matrix is filled with nearly pure aluminum, helping to diminish the thermal stress during accelerated solidification. Primary solidified silicon was found, however, containing considerable amounts of aluminum, which was not expected from phase diagrams obtained at the thermodynamic equilibrium.

**Keywords:** hypereutectic aluminum alloy; DISPAL; laser welding; nonequilibrium solidification

## 1. Introduction

Aluminum is a lightweight construction material possessing sufficient strength for many applications in automotive industries. Multiple alloying elements can influence and tailor the properties in a wide range. Silicon, for example, improves the wear resistance without increasing the density considerably. However, usually the weldability of aluminum alloys is influenced by the temperature range of solidification, and hot cracks are formed due to thermal shrinkage [1].

To take advantage of the improved properties of aluminum materials with very high silicon contents, spray-compacting is a process for the manufacturing of nonequilibrium materials with improved mechanical and tribological properties [2,3]. Alloys not producible by conventional casting processes can be made by spray-compacting at high temperature gradients of more than 1000 K/s during solidification. Insoluble alloying components can be distributed homogeneously in a matrix material since only small amounts hit a cold substrate and solidify rapidly. Indirect rod extrusion for compaction and occurring phases is described in [4]. These materials are known, e.g., under the

trade name DISPAL™ and are supplied by Erbslöh Aluminium GmbH in different compositions and conditions.

However, the question arises of how these materials can be joined since the dimension of semi-finished products is limited. In the literature, special welding techniques like friction stir welding are described, avoiding the formation of a liquid and segregation of nonequilibrium phases [5,6]. Therefore, laser welding could be an additional welding technique preserving the nonequilibrium state of the microstructure due to its high welding velocity. Especially since the development of multi-kilowatt solid state lasers and decreasing investment costs, laser welding has become widespread in, for example, the automotive industries [7–9].

Additionally, for many applications, a huge increase in productivity could be obtained by laser welding due to its high welding velocities, e.g., it replaces spot welding and fixes many issues combined with reduced heat input per unit of length.

In this paper, different hypereutectic Al-Si alloys were investigated at welding velocities between 0.5 to 10 m/min using a 3 kW disc laser to supply an additional joining technique to stir friction welding with high velocities. Changes in morphology and composition of occurring phases are discussed in respect to nonequilibrium conditions. The mechanical and especially the dynamic durability of welded parts made of hypereutectic Al-Si-alloys will depend on the size and number of precipitations in the microstructure of the weld seam. Welding parameters should be optimized to obtain small precipitations and to prevent the formation of pores. This is supported by high welding speeds and accelerated solidification of the weld pool.

## 2. Materials and Methods

### 2.1. Materials Used and Sample Preparation

Hypereutectic spray-compacted Al-Si-alloys were chosen by different silicon contents and additional alloying elements (see Table 1). The material was obtained by Erbslöh Aluminium GmbH as round stock of different diameters. Discs, approximately 10 mm in thickness, were cut using a BRILLANT 250 by ATM cutting machine (Mammelzen, Germany) with a 300 mm disk, type C with a thickness of 2 mm. Then, both sides of the samples were grinded using grained abrasive paper with 600 meshes per square inch in the SAPHIR 550 grinding machine by ATM (Mammelzen, Germany).

**Table 1.** Composition of DISPAL-alloys used for laser welding [10].

| Alloy | Composition | Si (wt. %) | Fe (wt. %) | Ni (wt. %) | Cu (wt. %) | Mg (wt. %) | Zr (wt. %) | Co (wt. %) | Ti (wt. %) | Al |
|-------|-------------|------------|------------|------------|------------|------------|------------|------------|------------|-----|
| S220 | AlSi35 | 35 | | | | | | | | balance |
| S225 | AlSi35Fe2Ni | 35 | 2 | 1 | | | | | | balance |
| S232 [11] | AlSi17Fe4Cu2.5MgZr | 17 | 4 | | 3 | 1 | <1 | | | balance |
| S263 | AlSi25Fe2.5Cu2.5Ni2.5MgCo | 25 | 3 | 3 | 3 | 1 | | 1 | 1 | balance |

### 2.2. Experimental Procedure

For laser welding, a TruCell 3010 machine and a TruDisk 3001 solid state disc laser by TRUMPF (Ditzingen, Germany) were combined. A light conducting cable (LCC) 100 μm in diameter was used to transfer the laser radiation from the disk laser to the machine tool. The optics had a focal length of 150 mm.

For the cross-section of a laser weld seam, the focal position of the focal spot may have a huge impact: To avoid the formation of pores, the energy density at the surface level must be sufficient to prevent solidification here first. Especially for small LCC-diameters the variation of the spot area at the surface level for a given focal position, in regards to the focal length, is more pronounced than for larger LCC-diameters.

Tests showed that different operators set the focal position using the image of a CCD-camera within a z-range of about 1.6 mm. Hence, a distance ruler was used to adjust the focal position related to the surface of the work piece (Figure 1). A focal position of $F = 0$ mm was used for all experiments.
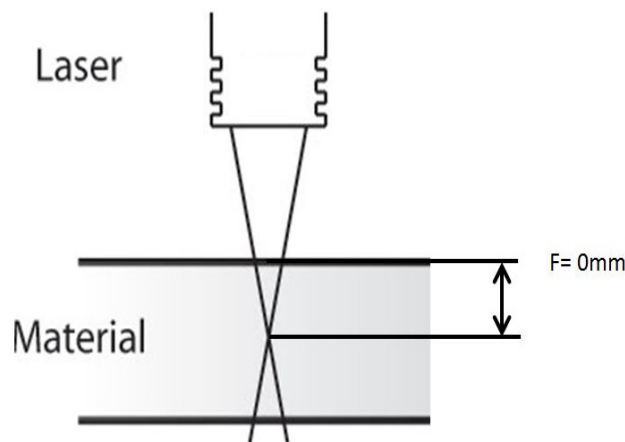


**Figure 1.** Focal position and its impact on the energy density at the surface, depending on the focal length.

All welding experiments were performed using 15 L/min of Ar 5.0. The inert gas supply was adjusted for backhand welding to shield from the melting bath. A length of 30 mm was welded for each welding velocity at a focal position of $F = 0$ mm using the maximum power of 3 kW.

Afterwards, the samples were cut perpendicular to the weld seams into two halves using the cutting machine BRILLANT 250. Both parts were hand grinded starting at 600 meshes per square inches down to 2400 abrasive paper using the SAPHIR 550 grinding machine, and polished using monocrystalline diamond suspension of 9, 6 and 1 µm, respectively.

From Figure 2, the impact of the welding speed on the cross-section can be seen: For low welding speed, the deepest weld seams were obtained; however, also the width at the surface is high due to slow solidification and heat conduction. For high welding speeds, narrower weld seams at reasonable welding depths are possible.
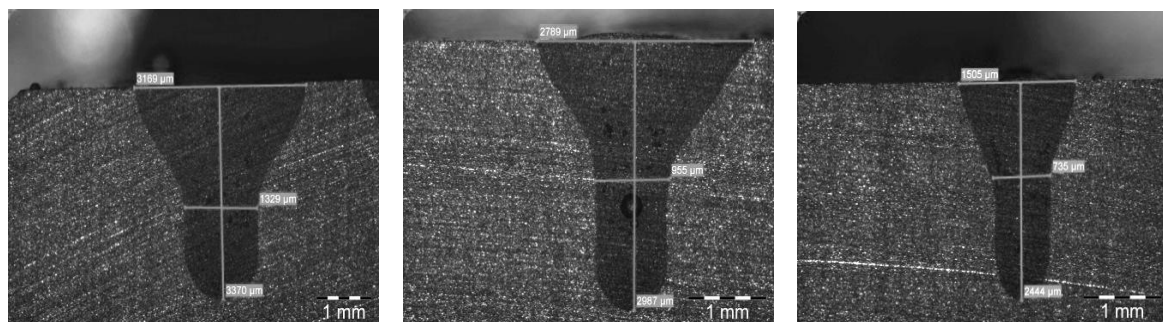


**Figure 2.** From **left** to **right**: Cross-section views for DISPAL S220 for welding velocities of 3, 5 and 10 m/min for $P = 3$ kW and a focal position of $F = 0$ mm. For 3 m/min the positions of EDX measurements are marked for base material, transition zone and weld seam.

Photographs were taken using a stereomicroscope SZX12 by OLYMPUS, Hamburg, Germany. SEM pictures were taken by a JSM 6300 by JEOL (Freising, Germany) at different spots of the weld seams. A microprobe JXA 8530F by JEOL (Freising, Germany) with field emitting cathode was used for EDX and WDX investigations. For EDX a voltage of 15 kV, a working distance of 11 mm and a current of 1.5 nA to ensure a count rate of at least 2500 count/s were used.

## 3. Results and Discussion

### *3.1. Microstructure of Spray-Compacted and Welded DISPAL-Alloys*

As expected, primary silicon precipitations in the delivery condition of all materials are globular and uniformly distributed all over the matrix for all kinds of materials. In laser-welded areas, however, spiky precipitations are generally observed according to the local solidification rate. Additionally, depending on the welding velocity, a network of near-eutectic composition is formed, embedding inclusions of nearly pure aluminum.

SEM pictures were taken in the transition section to the base material as well as in the center of the weld seam. EDX measurements were performed in the middle of the weld seams at a depth where the funnel-shaped area changes to a straight one, representing the lowest solidification velocity.

Whereas the compositions in all tables are given in percent by weight, the evaluation of the results refers to percent by atom to recognize phase compositions. In case of aluminum and silicon, the differences between both are small; however, for metals with higher atomic number, e.g., iron, nickel and copper, distinction is obvious.

From Figure 3 it can be seen that the solubility of silicon in aluminum is very low and iron is not soluble in silicon. For other DISPLA-alloys containing up to five additional elements, the conditions concerning solubility and formation of intermetallic compounds are conspicuous.
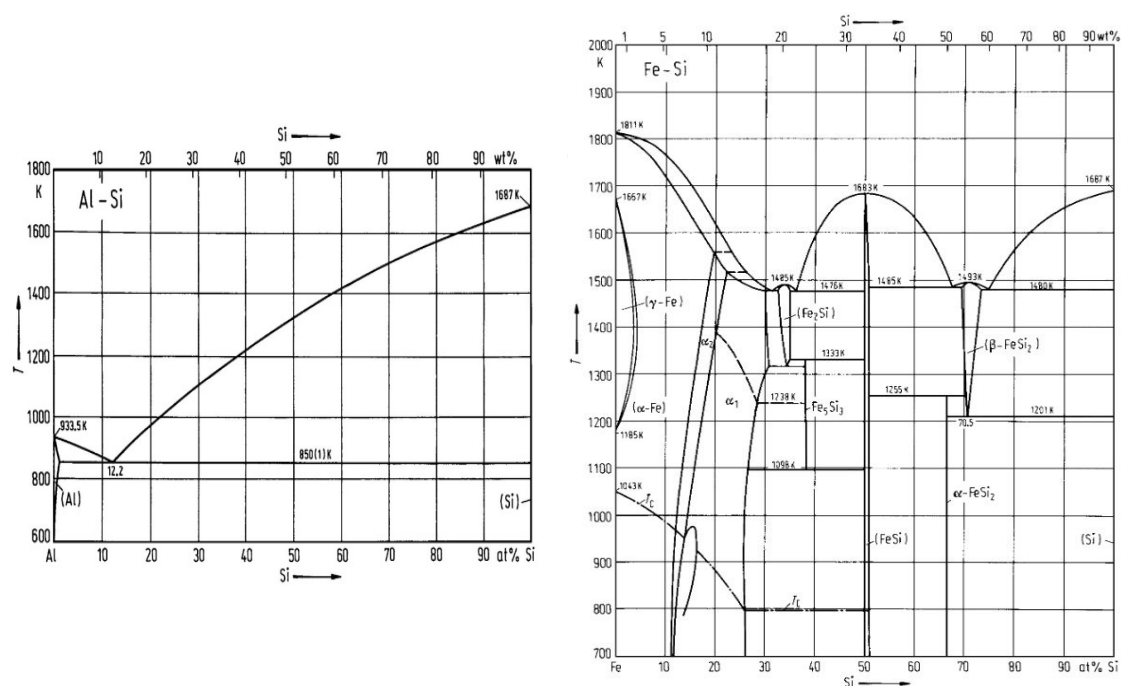


**Figure 3.** Binary phase diagrams of Si-Al (**left**) and Si-Fe (**right**) [12].

Figures 4, 6, 8 and 10 show four different SEM pictures of all materials at different spots according to the increasing silicon content of the alloys: top left of the original base material; top right the transition zone of the weld seam to the base material; and below the microstructure in the center of the weld seams for welding velocities of 0.5 and 10 m/min, respectively. All pictures for the transition zone were taken from the 10 m/min weld seam due to a more pronounced and narrower crossover. For 0.5 m/min, however, the transition was more blurred.

*3.2. DISPAL S220: Comparision of Comosition Measured by WDX and EDX*

In Figure 4, SEM pictures of S220 with the highest silicon content of 35 wt. % without additional alloying elements are shown. Some small bright precipitations are found, probably due to impurities by other elements originating from impurities of the recycled material.

Compared to other alloys, coarser and predominantly silicon-containing precipitations are observed.
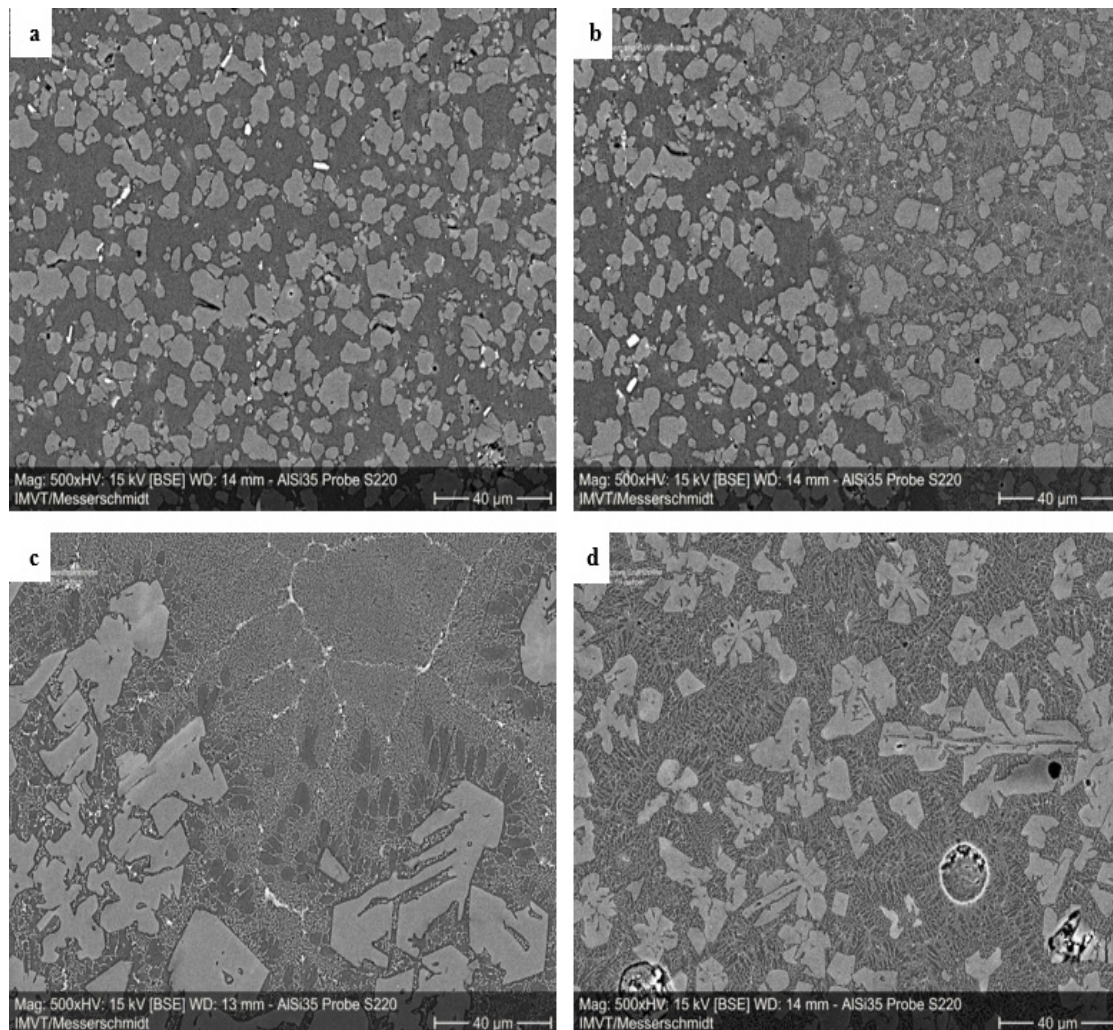


**Figure 4.** S220: (**a**) Base material; (**b**) Transition of weld seam to base material; (**c**) Center of the weld seam for $v$ = 0.5 m/min; (**d**) Center of the weld seam for $v$ = 10 m/min.

Light elements like carbon or oxygen may be overestimated by EDX since its specific energy is superimposed to the "bremsstrahlung". Hence, citing S220 as an example, WDX was employed for a welding speed of 0.5 m/min to test if the content of oxygen measured by EDX (Table 2) is in a reliable range. The results in wt. % obtained from measurements employing elemental standards showed a deviation within ±1% to 100% for different sample points. For Table 3, the values were scaled to 100% and given in at. %. From this it can be concluded that the values of oxygen content obtained by EDX for other samples are reasonable. All alloys contain noticeable amounts of oxygen, in the base material as well as in the weld seams, likely from passivation layers and impurities during spray-compacting. A significant increase of oxygen content from as-delivered condition and welded material is not detected.

**Table 2.** Composition of S220 measured using EDX for a welding speed of 0.5 m/min (at. %).

| Spot | No. | Al | Si | Fe | Cu | O | Suggested Phase |
|------|-----|-----|-----|-----|-----|-----|-----------------|
| Base mat. | 1 | 96.8 | 1.57 | 0.18 | 0.01 | 1.45 | |
| | 2 | 53.89 | 44.63 | 0.2 | / | 1.28 | |
| | 3 | 1.55 | 96.66 | 0.03 | 0.08 | 1.69 | |
| | 4 | 1.55 | 96.66 | 0.03 | 0.08 | 1.69 | |
| | 5 | 86.38 | 12.02 | 0.01 | 0.03 | 1.56 | eutectic |
| | 6 | 93.37 | 4.39 | 0.05 | 0.14 | 2.51 | |
| Welding speed 0.5 m/min | 1 | 90.0 | 7.93 | 0.44 | 0.04 | 1.59 | |
| | 2 | 86.26 | 11.09 | 0.94 | 0.1 | 1.61 | eutectic |
| | 3 | 3.31 | 95.58 | 0.12 | / | 0.99 | |
| | 4 | 41.65 | 57.29 | / | / | 1.06 | |
| | 5 | 68.21 | 29.31 | 0.04 | 0.14 | 2.29 | |
| | 6 | 92.6 | 5.92 | 0.02 | 0.07 | 1.4 | |
| Welding speed 10 m/min | 1 | 77.47 | 20.07 | 0.53 | 0.14 | 1.8 | |
| | 2 | 74.79 | 20.66 | 0.93 | 0.15 | 3.46 | |
| | 3 | 1.77 | 97.11 | 0.05 | 0.03 | 1.04 | |
| | 4 | 2.99 | 95.82 | / | 0.19 | 1.0 | |
| | 5 | 85.33 | 12.45 | 0.35 | / | 1.87 | eutectic |
| | 6 | 78.95 | 18.92 | 0.05 | 0 | 2.08 | |

**Table 3.** Composition of S220 measured by WDX for a welding speed due to 0.5 m/min (at. %).

| Spot/Phases | | No. | Al | Si | Fe | Cu | O |
|-------------|--|-----|-----|-----|-----|-----|-----|
| Base mat. | "bright" phase | 1 | 2.80 | 96.53 | 0.02 | 0.01 | 0.64 |
| | | 2 | 2.22 | 97.53 | 0.00 | 0.01 | 0.24 |
| | | 3 | 3.20 | 96.45 | 0.01 | 0.01 | 0.34 |
| | | 4 | 1.27 | 98.20 | 0.01 | 0.01 | 0.51 |
| | | 5 | 1.56 | 97.98 | 0.00 | 0.02 | 0.45 |
| | "dark" phase | 1 | 98.57 | 0.22 | 0.01 | 0.02 | 1.18 |
| | | 2 | 98.20 | 0.24 | 0.01 | 0.01 | 1.53 |
| | | 3 | 97.44 | 0.85 | 0.23 | 0.00 | 1.48 |
| | | 4 | 98.30 | 0.32 | 0.01 | 0.01 | 1.36 |
| | | 5 | 98.41 | 0.26 | 0.00 | 0.01 | 1.32 |
| Welding speed 0.5 m/min | "bright" phase | 1 | 2.76 | 96.91 | 0.01 | 0.00 | 0.32 |
| | | 2 | 3.25 | 96.24 | 0.01 | 0.01 | 0.50 |
| | | 3 | 2.68 | 96.82 | 0.00 | 0.00 | 0.51 |
| | | 4 | 3.71 | 95.78 | 0.00 | 0.00 | 0.51 |
| | | 5 | 2.88 | 96.60 | 0.00 | 0.00 | 0.52 |
| | "dark" phase | 1 | 81.74 | 16.03 | 0.02 | 0.04 | 2.17 |
| | | 2 | 87.73 | 10.67 | 0.14 | 0.06 | 1.40 |
| | | 3 | 86.67 | 11.90 | 0.01 | 0.01 | 1.41 |
| | | 4 | 80.29 | 17.90 | 0.00 | 0.00 | 1.81 |
| | | 5 | 79.16 | 17.62 | 0.03 | 0.02 | 3.16 |

EDX measurements showed for the base material as well as the weld seams in Figure 5 and Table 2 that the precipitations consist mainly of silicon for more than 95 at. %. The silicon content in the aluminum matrix of the base material is 12 and 4.4 at. % for No. 5 and 6, respectively, making it difficult to derive a statement about the influence of the solidification speed on the silicon content in the supersaturated aluminum matrix.

It is noteworthy that the silicon content in the eutectic network for 10 m/min (No. 1, 2 and 6) is around 19–20 at. %. Globular grey islands (No. 5) are embedded, having exactly the eutectic composition of 12.5 at. % without the typically lamellar segregation. For 0.5 m/min, however, the silicon content in the matrix (No. 5) is 6 at. %, but the influence of welding velocity on the segregation of silicon from a homogeneous melt cannot be surely stated due to contradictory results from the base material.

Additionally, pearl-shaped, small precipitations forming a loose network are formed for 0.5 m/min. For 10 m/min, however, their size is clearly much smaller due to faster solidification and

insular areas. The composition is difficult to determine due to the small size for both welding speeds. It seems to contain impurities of iron and copper.
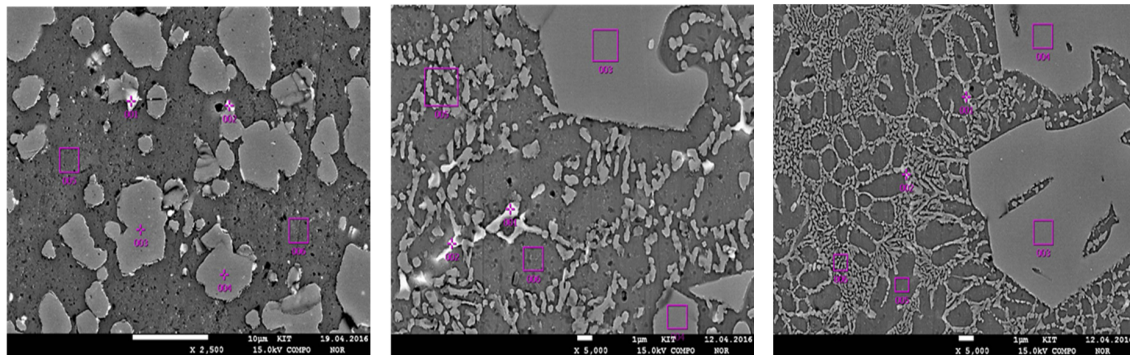


**Figure 5.** EDX investigation of phases in S220: **Left**: base material; **Middle**: welding speed 0.5 m/min; **Right**: welding speed 10 m/min.

## 3.3. Microstructures of DISPAL-Alloys Containing Additional Alloying Elements

### 3.3.1. DISPAL S225

In contrast to S220, for S225, 2 wt. % of iron and about 1 wt. % of nickel are added. This alloy was chosen to evaluate differences in phase compostion and morphology in relation to S220.
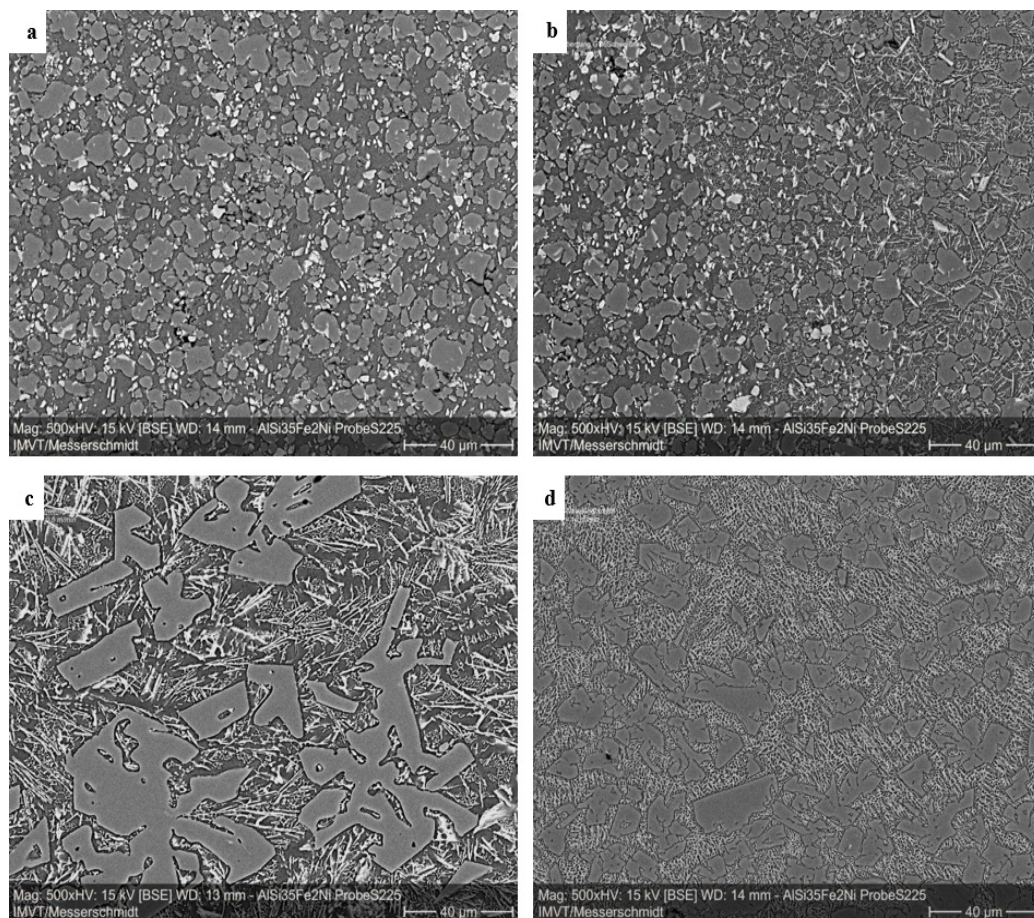


**Figure 6.** S225. (**a**) Base material; (**b**) Transition of weld seam to base material; (**c**) Center of the weld seam for $v$ = 0.5 m/min; (**d**) Center of the weld seam for $v$ = 10 m/min.

Actually, as shown in Figure 7, already in the base material more bright precipitations containing metals of higher atomic number are found. Shape and size of silicon-rich precipitations are similar to S220. However, in the weld seam, the morphology of the precipitation network is changed drastically: iron and nickel change the shape of bright precipitations between the large, primary silicon-rich precipitations from pearl-like to spicular, even for the low welding speed of 0.5 m/min. From the EDX-investigations in Figure 7 and Table 4, it can be seen that iron is concentrated in these spicular precipitations. The distance between these spicular precipitations decrease considerably for 10 m/min welding speed, whereas the size of primary silicon-rich precipitations is only slightly affected. Especially the microstructure for 10 m/min should have favorable mechanical properties due to its homogeneous distribution of the precipitations.
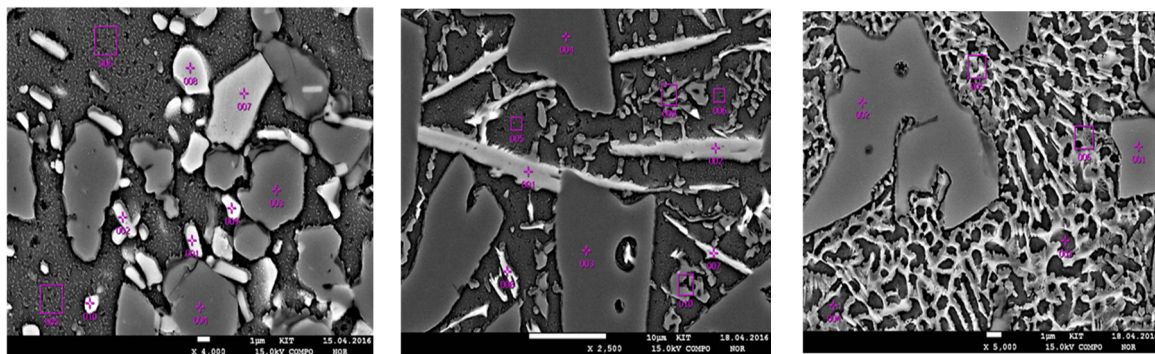


**Figure 7.** EDX investigation of phases in S225: **Left**: base material; **Middle**: welding speed 0.5 m/min; **Right**: welding speed 10 m/min.

**Table 4.** Composition of S225 measured by EDX (at. %).

| Spot | No. | Al | Si | Fe | Ni | Mg | O |
|---|---|---|---|---|---|---|---|
| | 1 | 54.44 | 30.79 | 9.35 | 0.73 | 0.18 | 4.51 |
| | 2 | 51.67 | 34.29 | 8.43 | 0.83 | 0.08 | 4.69 |
| | 3 | 12.53 | 85.83 | 0.28 | 0.18 | 0.12 | 1.06 |
| | 4 | 4.47 | 93.32 | 0.17 | 0.21 | / | 1.83 |
| Base mat. | 5 | 96.64 | 0.73 | 0.18 | / | 0.22 | 2.23 |
| | 6 | 96.73 | 0.56 | 0.14 | 0.12 | 0.17 | 2.28 |
| | 7 | 66.64 | 3.03 | 6.61 | 8.59 | 0.1 | 15.04 |
| | 8 | 65.42 | 3.29 | 7.4 | 10.88 | 0.05 | 12.97 |
| | 9 | 72.09 | 14.56 | 4.77 | 5.91 | 0.04 | 2.63 |
| | 10 | 93.6 | 1.45 | 1.0 | 1.24 | 0.18 | 2.54 |
| | 1 | 64.92 | 20.58 | 10.89 | 1.41 | 0.05 | 2.15 |
| | 2 | 81.27 | 10.67 | 5.15 | 0.67 | 0.21 | 2.03 |
| | 3 | 0.94 | 97.92 | 0.07 | 0.21 | 0.06 | 0.8 |
| | 4 | 1.49 | 97.29 | / | / | 0.02 | 1.2 |
| Welding speed | 5 | 95.02 | 2.83 | 0.22 | 0.05 | 0.11 | 1.76 |
| 0.5 m/min | 6 | 90.83 | 6.54 | 0.2 | 0.32 | 0.19 | 1.91 |
| | 7 | 93.33 | 3.99 | 0.96 | 0.14 | 0.03 | 1.55 |
| | 8 | 77.56 | 11.7 | 6.59 | 2.37 | 0.3 | 1.47 |
| | 9 | 69.11 | 28.33 | 0.15 | 0.05 | 0.13 | 2.22 |
| | 10 | 64.49 | 33.5 | 0.1 | / | 0.08 | 1.83 |
| | 1 | 4.67 | 93.47 | 0.14 | 0.18 | 0.02 | 1.53 |
| | 2 | 5.95 | 92.96 | 0.02 | 0.01 | 0.02 | 1.04 |
| Welding speed | 3 | 80.61 | 11.66 | 2.5 | 1.04 | 0.23 | 3.97 |
| 10 m/min | 4 | 80.36 | 12.6 | 1.78 | 0.86 | 0.07 | 4.33 |
| | 5 | 69.58 | 22.39 | 2.78 | 0.83 | 0.18 | 4.29 |
| | 6 | 67.03 | 26.36 | 1.46 | 0.57 | 0.12 | 4.46 |

### 3.3.2. DISPAL S232

For S232 in Figure 8, it can be seen that there are different globular precipitations in the base material rich in silicon and iron. Compared to the other alloys, the content of precipitations corresponds to the silicon content.
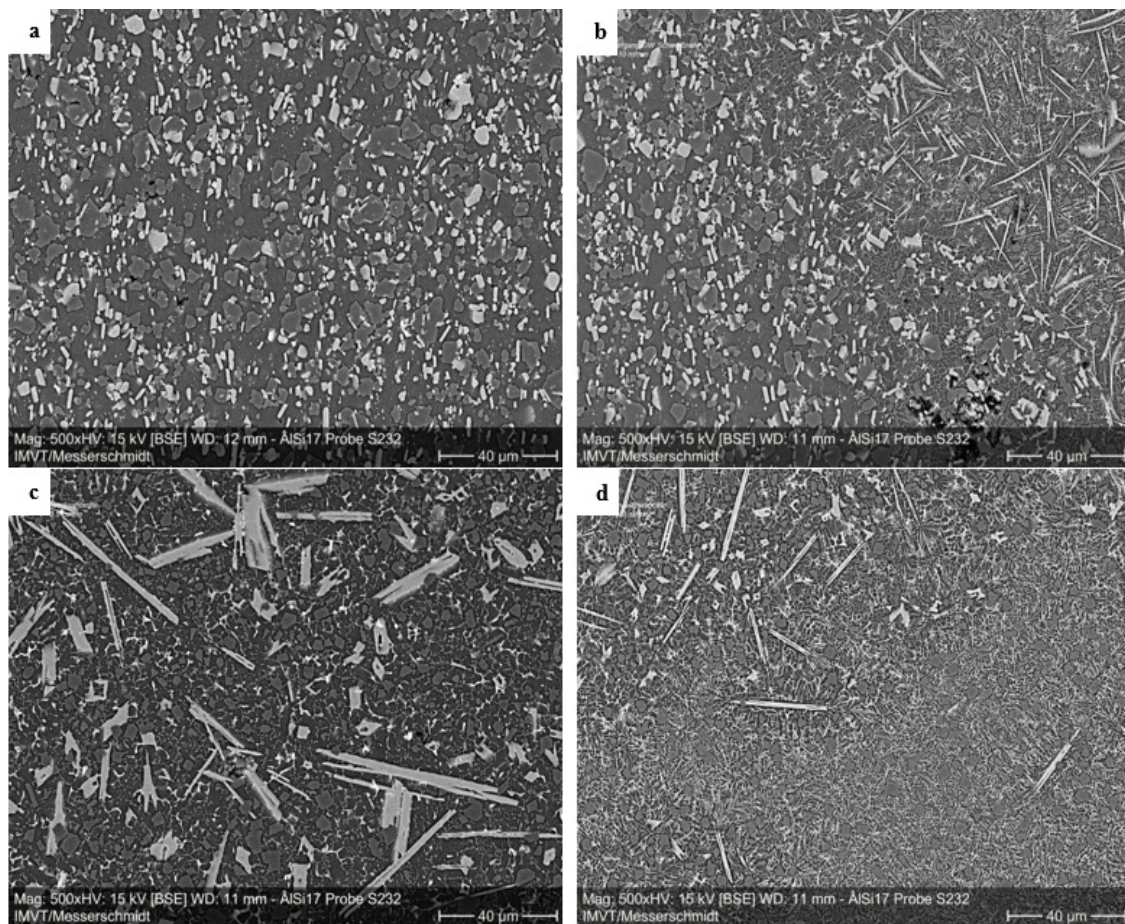


**Figure 8.** S232: (**a**) Base material; (**b**) Transition of weld seam to base material; (**c**) Center of the weld seam for $v$ = 0.5 m/min; (**d**) Center of the weld seam for $v$ = 10 m/min.

In the transition area, the morphology of the matrix is already changed to network-like meshes, pointing to a near-eutectic phase, whereas the globular silicon precipitations still exist.

The alloying elements are solved in the melting bath and new precipitations, at least differently shaped ones, are formed. Inside the weld seams for welding velocities of 0.5 and 10 m/min, respectively, grey angular precipitations are visible, similar to the matrix, although smaller in size. Bright spicular precipitations, containing most of the iron and copper, are formed. Length and thickness of these precipitations seem to grow for lower welding speeds since the solidification is retarded in relation to high velocities.

In between with increasing welding speed, as matrix an eutectic microstructure is developed [4]. However, zirconium forming Al3Zr-dispersoids could not be found in this alloy (Table 5).

In any case, these different phases solidifying at different temperatures and maintaining short distances in between help to reduce thermal contraction strains and to avoid hot cracks as known for alloys with a wide solidification range like for some aluminum alloys.

**Table 5.** Composition of S232 measured by EDX for a welding speed of 0.5 m/min (at. %).

| Spot | No. | Al | Si | Fe | Cu | Mg | O | Suggested Phase |
|------|-----|-----|-----|-----|-----|-----|-----|-----------------|
| Base mat. | 1 | 68.31 | 14.25 | 11.49 | 0.77 | 0.2 | 4.97 | Al5FeSi |
| | 2 | 87.33 | 3.94 | 1.42 | 2.11 | 0.46 | 4.74 | |
| | 3 | 12.82 | 84.24 | 0.69 | 0.3 | 0.1 | 1.85 | |
| | 4 | 42.64 | 53.8 | 0.14 | 0.76 | 0.2 | 2.46 | |
| | 5 | 87.8 | 4.15 | 2.0 | 1.6 | 0.55 | 3.90 | |
| | 6 | 91.29 | 1.64 | 0.25 | 1.97 | 0.64 | 4.21 | |
| | 7 | 65.01 | 16.91 | 14.32 | 0.35 | 0.11 | 3.3 | Al5FeSi |
| | 8 | 81.52 | 12.53 | 0.25 | 2.01 | 0.59 | 3.08 | |
| Welding speed 0.5 m/min | 1 | 67.23 | 14.17 | 14.85 | 0.07 | 0.03 | 3.66 | |
| | 2 | 71.47 | 13.04 | 11.2 | 0.77 | 0.14 | 3.38 | |
| | 3 | 5.72 | 92.06 | 0.14 | 0.26 | 0.1 | 1.71 | |
| | 4 | 28.93 | 68.92 | 0.1 | 0.16 | 0.24 | 1.64 | |
| | 5 | 74.76 | 22.1 | 0.13 | 0.92 | 0.47 | 1.62 | |
| | 6 | 85.76 | 5.2 | 0.33 | 4.99 | 0.56 | 3.17 | |
| | 7 | 63.85 | 6.23 | 1.74 | 12.76 | 1.57 | 13.84 | |
| | 8 | 86.29 | 3.62 | 0.59 | 3.25 | 0.89 | 5.36 | |
| | 9 | 65.05 | 30.93 | 0.24 | 0.62 | 0.29 | 2.89 | |
| | 10 | 77.48 | 18.72 | 0.25 | 0.91 | 0.43 | 2.21 | |
| Welding speed 10 m/min | 1 | 58.84 | 23.81 | 12.03 | 1.65 | 0.39 | 3.28 | |
| | 2 | 67.61 | 13.81 | 14.0 | 0.57 | 0.4 | 3.61 | |
| | 3 | 27.24 | 71.02 | 0.23 | 0.19 | 0.16 | 1.16 | |
| | 4 | 31.96 | 65.39 | 0.38 | 0.29 | 0.19 | 1.8 | |
| | 5 | 71.58 | 24.63 | 0.31 | 0.68 | 0.42 | 2.38 | |
| | 6 | 71.43 | 23.66 | 1.12 | 0.81 | 0.6 | 2.38 | |
| | 7 | 83.34 | 6.94 | 2.06 | 4.31 | 1.17 | 2.17 | |
| | 8 | 76.43 | 14.48 | 1.84 | 2.06 | 1.32 | 3.87 | |

EDX-investigations were done at different spots for the different phases in the base material as well as inside the weld seams. Figure 9 gives an overview of the morphologies and the spots where the composition was determined. Noteworthy is the higher magnification for the SEM-picture for 10 m/min welding speed, indicating a finer microstructure than for 0.5 m/min. In the base material, three compositions of precipitations different in phase contrast were found: bright particles, e.g., No. 1, 2, 7 and 8 of the left picture of Figure 9, respectively, contain nearly the whole amount of iron and copper. No. 1 and 7 corresponds to the intermetallic phase Al5FeSi, mentioned in [4]. For ternary or quaternary alloys, even more complex phases are reported, e.g., in [13]. Darker precipitations, e.g., No. 3 and 4, contain silicon in excess of the eutectic composition. The matrix, however, for No. 5 and 6, consists mainly of aluminum with some iron and copper, in which copper is soluble in aluminum and iron is not.
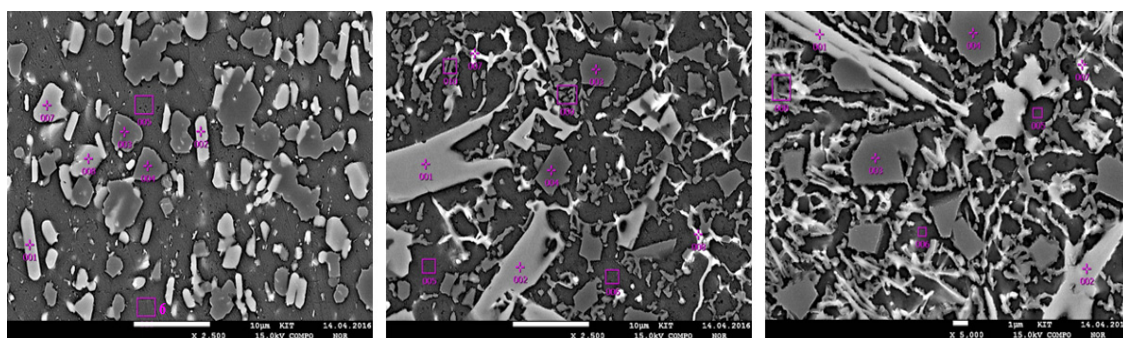


**Figure 9.** EDX investigation of phases in S232: **Left**: base material; **Middle**: welding speed 0.5 m/min; **Right**: welding speed 10 m/min.

For the weld seams, the composition of the precipitations is maintained despite different species in terms of aluminum and silicon can be found. The silicon content in the matrix, however, rises from less than 5 at. % for more than 20 at. %. The bright network contains about 6 at. % silicon, 2 at. % iron and copper between 4.3 and 12.8 at. % copper (No. 7 for 0.5 and 10 m/min, respectively). No. 8 for 0.5 m/min, however, contains much more aluminum. Probably it is due to the small dimension of the network, so the measurement is affected by the material below.

### 3.3.3. DISPAL S263

In Figure 10, for the base material, there are more precipitation—albeit less bright—corresponding to the higher silicon content of 25 wt. %. In the weld seams, the network in the matrix is more developed than for S232 due to the higher silicon content, forming an eutectic phase. Obviously, the dark precipitations for 0.5 m/min welding speed are larger than for 10 m/min, in contradiction to S232, and bright precipitations containing metals with higher atomic numbers are thicker than for 10 m/min.
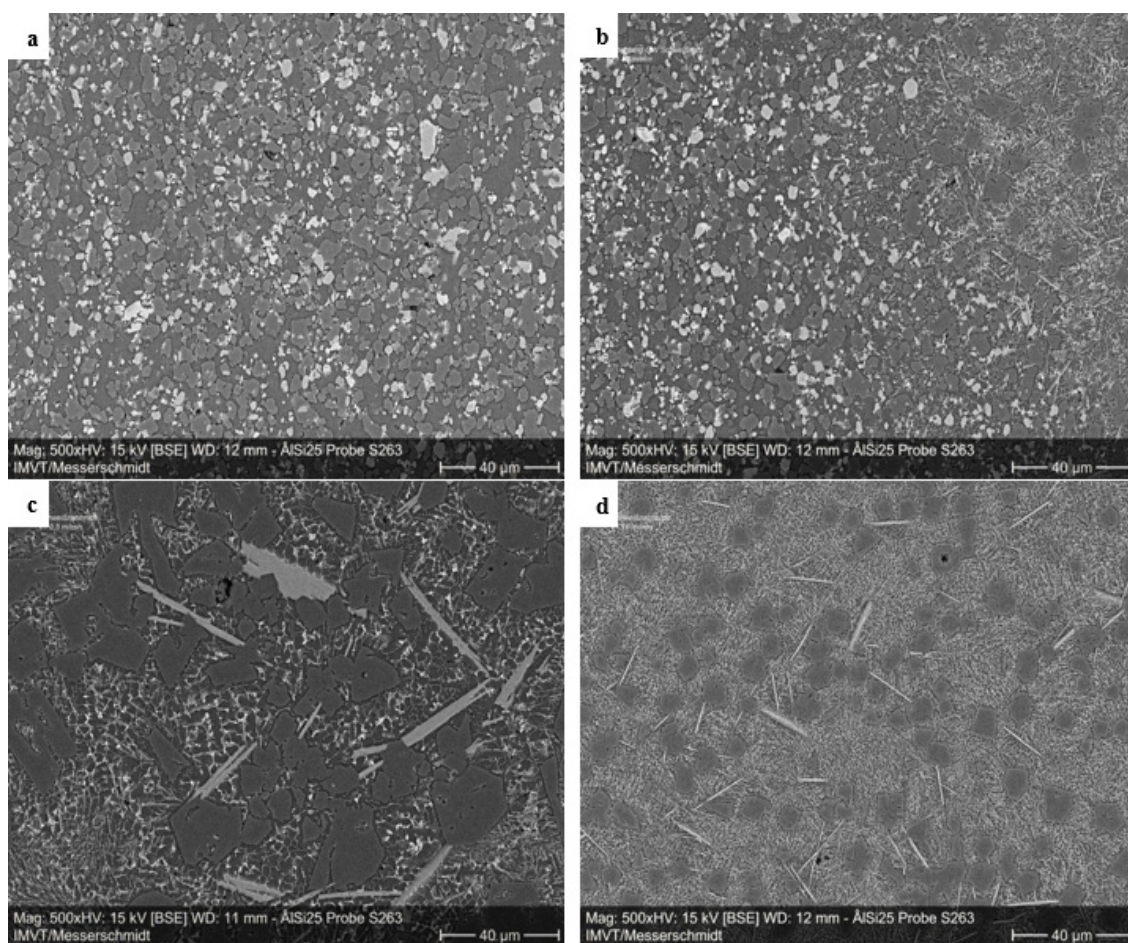


**Figure 10.** S263: (**a**) Base material; (**b**) Transition of weld seam to base material; (**c**) Center of the weld seam for $v$ = 0.5 m/min; (**d**) Center of the weld seam for $v$ = 10 m/min.

Different phases were investigated as shown in Figure 11 and Table 6, respectively. Whereas the silicon content inside the dark precipitations in the base material are between 84.5 and 76 at. %, for No. 3 and 4, respectively, the silicon content in these precipitations in the weld seams is higher than 90 at. % (same numbers as for the base material). Again, the precipitations are a little larger for the lower speed. Whereas the bright precipitation (No. 1 and 2 for both welding speeds) for 0.5 m/min contains about 24 at. % silicon, 11 to 14 at. % iron, about 0.5 at. % copper and 2.1 to 2.6 at. % nickel,

the silicon content for 10 m/min is near-eutectic between 8.5 and 11.9 at. % and iron, nickel and copper are around 1 at. %.

**Table 6.** Composition of S263 measured by EDX for a welding speed of 0.5 m/min (at. %).

| Spot | No. | Al | Si | Fe | Co | Ni | Cu | Mg | O | Suggested Phase |
|------|-----|-----|-----|-----|-----|-----|-----|-----|-----|-----------------|
| Base mat. | 1 | 73.05 | 5.76 | 9.11 | 1.15 | 7.16 | 0.54 | 0.11 | 3.13 | |
| | 2 | 76.86 | 4.83 | 7.43 | 0.64 | 5.8 | 0.89 | 0.11 | 3.44 | |
| | 3 | 12.88 | 84.65 | 0.32 | 0.01 | 0.32 | 0.47 | 0.11 | 1.23 | |
| | 4 | 22.7 | 75.92 | 0.18 | 0 | 0.12 | 0.16 | 0.02 | 0.89 | |
| | 5 | 94.61 | 1.61 | 0.27 | 0.02 | 0.05 | 0.87 | 0.19 | 2.37 | |
| | 6 | 90.19 | 6.49 | 0.12 | 0.02 | 0.27 | 0.8 | 0.27 | 1.84 | |
| Welding speed 0.5 m/min | 1 | 57.49 | 23.78 | 10.94 | 0.91 | 2.61 | 0.17 | 0.05 | 4.03 | Fe2Al3Si3? |
| | 2 | 55.3 | 25.63 | 13.91 | 0.89 | 2.1 | 0.34 | 0.11 | 1.76 | Fe2Al3Si3? |
| | 3 | 1.12 | 96.86 | 0.03 | 0.05 | 0.13 | 0.29 | / | 1.5 | |
| | 4 | 2.67 | 95.33 | 0.07 | / | 0.18 | 0.19 | / | 1.56 | |
| | 5 | 77.65 | 13.88 | 1.3 | 0.1 | 1.53 | 1.42 | 0.8 | 3.32 | |
| | 6 | 85.9 | 10.76 | 0.22 | 0.01 | 0.08 | 0.7 | 0.25 | 2.08 | |
| | 7 | 80.93 | 11.99 | 2.13 | 0.21 | 1.63 | 0.9 | 0.7 | 1.5 | |
| | 8 | 83.07 | 8.98 | 0.21 | 0.02 | 1.78 | 2.96 | 0.35 | 2.63 | |
| Welding speed 10 m/min | 1 | 85.95 | 8.47 | 1.15 | 0.07 | 0.9 | 0.86 | 0.48 | 2.12 | |
| | 2 | 82.15 | 11.92 | 1.09 | 0.04 | 1.07 | 0.98 | 0.72 | 2.02 | |
| | 3 | 6.94 | 91.07 | 0.18 | 0.06 | 0.03 | 0.23 | 0.04 | 1.45 | |
| | 4 | 5.0 | 93.44 | 0.12 | 0.12 | 0.15 | 0.11 | 0.03 | 1.02 | |
| | 5 | 75.05 | 16.27 | 1.54 | 0.06 | 1.5 | 1.34 | 0.48 | 3.76 | |
| | 6 | 79.21 | 12.59 | 0.76 | 0.05 | 1.12 | 1.22 | 0.41 | 4.65 | |

The bright network (No. 7 for 0.5 m/min) is nearly eutectic with some content of iron, nickel and copper. For 10 m/min, the dimension is too small to determine the composition of the network. The matrix (No. 6 for both welding speeds) possesses near-eutectic composition without showing an additional lamellar microstructure at a smaller scale. It is likely that the silicon content is frozen in a supersaturated solid solution.
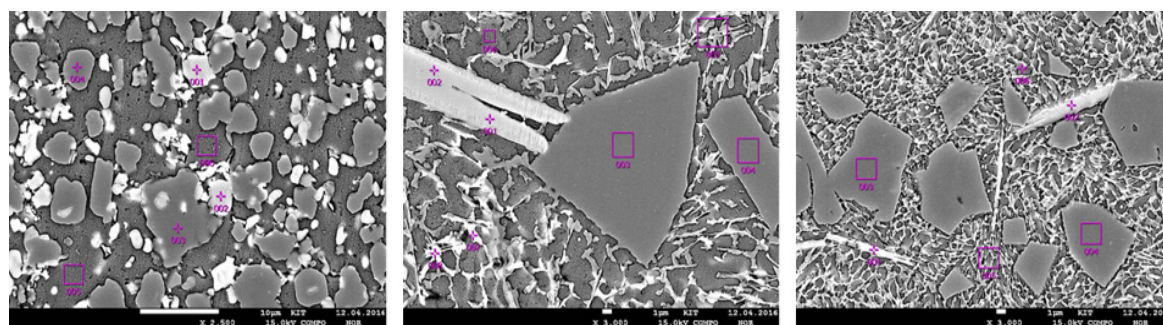


**Figure 11.** EDX investigation of phases in S263: **Left**: base material; **Middle**: welding speed 0.5 m/min; **Right**: welding speed 10 m/min.
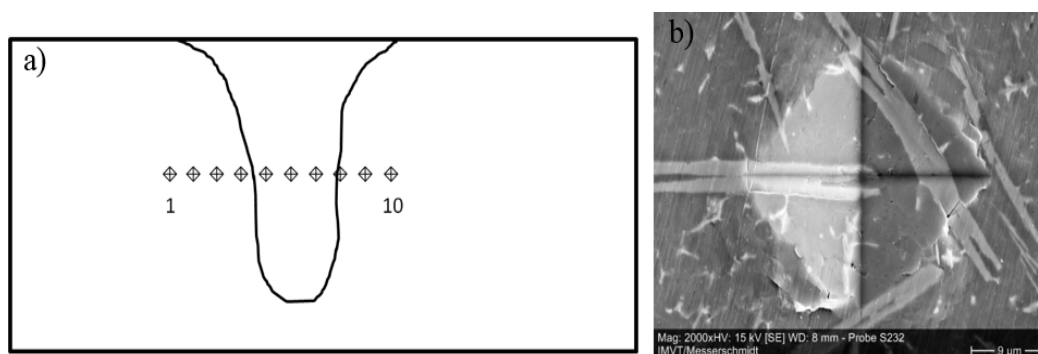
### 3.4. Micro Hardness Measurements

For S 225, S232 and S263, containing additional alloying elements except silicon, microhardness measurements were performed at weld seams at a velocity of 1 m/min. A Matsuzawa Model MMT-X7B and HV0.1, corresponding to a load of 0.98 N, was employed. The distance between single indentations was 0.5 mm. Different grey levels for background in Table 7 were used to distinguish between as-delivered conditions of spray-compacted materials, heat-affected zones and weld seams. Figure 12a

displays the schema of single indentations. Taking into account the scale of the inhomogeneity of the microstructure and the indentations, a certain variance of hardness values is plausible (Figure 12b).

**Table 7.** Microhardness measurements for S 225, S232 and S263. White background: base material, middle grey: heat-affected zone, dark: weld seam.

| Material | HV$_{0.1}$ | | | | | | | | | |
|---|---|---|---|---|---|---|---|---|---|---|
| S225 | 121 | 118 | 127 | 185 | 208 | 146 | 165 | 120 | 138 | 119 |
|  | 120 | 120 | 150 | 220 | 233 | 225 | 231 | 134 | 126 | 121 |
| S232 | 176 | 174 | 181 | 216 | 215 | 198 | 176 | 181 | 174 | 170 |
|  | 170 | 177 | 170 | 195 | 192 | 180 | 171 | 175 | 165 | 171 |
| S263 | 134 | 143 | 199 | 228 | 226 | 228 | 235 | 213 | 174 | 147 |



**Figure 12.** (**a**) Schema of microhardness measurements; (**b**) Detail of micro indentation.

For S225 and S232, two microhardness measurements were made at different depths, both in the area of constant width of the weld seam.

Despite the highest silicon content for S225 resulting in the highest density of silicon precipitations, the hardness of the spray-compacted matrix material is lowest. It is probable that the contribution of solid solution hardening is low since it contains only 2% iron, and because nickel is insoluble in aluminum. Inside the weld seam, higher microhardness values were obtained due to spicular and more homogeneous distributed precipitations.

For S232, containing higher contents of additional alloying elements contributing to solid solution hardening, a higher hardness of the as-delivered state is found. Since the silicon content is only half in comparison to S225, the precipitations are smaller. The microstructure appears finer than for S225, and hence microhardness values scatter less.

S263 has a silicon content of 25% and contains the highest amount and most alloying elements. Only for nickel is no solubility in aluminum found, and solubility for cobalt and titanium is very low. All metals form intermetallic compounds with aluminum. However, the content is possibly too low and solidification time during laser welding too short to reach these compositions and equilibrium conditions. Surprisingly, the microhardness of the as-delivered material is lower than for S232 but, in the weld seam, the hardness level is slightly increased compared to S232.

*3.5. X-ray Diffraction (XRD) Measurements of S263*

XRD measurements were performed using a Bruker D8 Discover with GADDS and a Hi-STAR area detector in reflection geometry. The sample to detector distance was 13.7 cm. A 500 μm pinhole collimator was used and the sample was oscillated with 1 mm steps to radiate a larger sample area. Cu-K$\alpha$-radiation was used and the exposure time was 30 min. Figure 13 shows spectra of as-delivered material and weld seam for a velocity of 1 m/min. Data were evaluated using an online database [14]. S263 contains seven elements and is a very complex system. Despite the obvious additional peaks, most could not be fitted to known intermetallic compounds. Additionally, the database PDF-2,

Release 2015, by the International Centre for Diffraction Data, containing more than 700 phases for the Al-Si-Fe-Ni-Cu-system, was used. Here, phases like Fe3Al2Si4 (PDF 1-087-1921), Al3FeSi2 (PDF 52-0917), AlCu3 (PDF 1-74-6895), Al5.4Fe2 (PDF 1-73-8846), Al5.6Fe2 (PDF 1-71-9849), NiSi (PDF 1-70-9169) and Ni31Si12 (PDF 17-222) were suggested; however, positions of specific reflexes are in poor accordance.
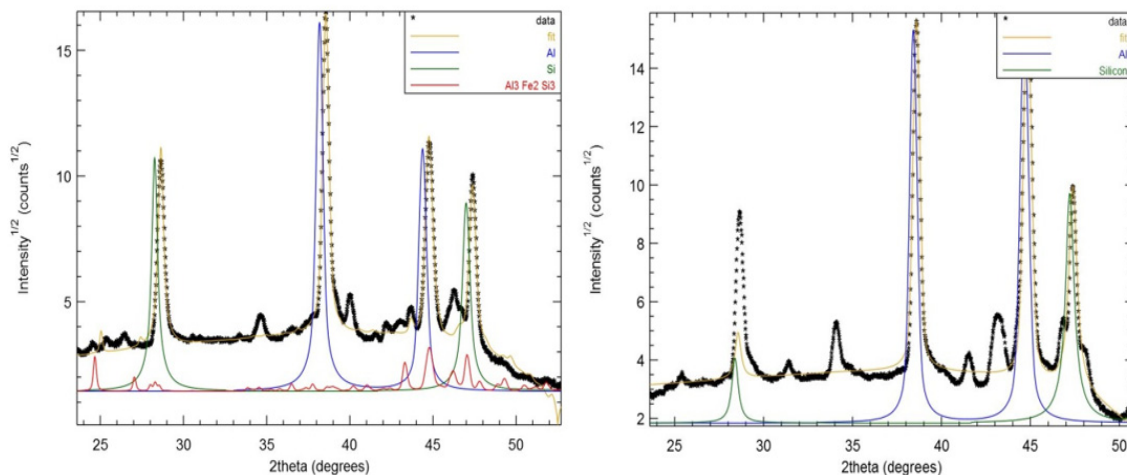


**Figure 13. Left**: XRD pattern of S263 as-delivered state; **Right**: As welded at 1 m/min.

Although the solidification rate for the weld seam should be lower and closer to thermodynamically equilibrium than for spray-compacted material, no additional intermetallic compound was found. However, one intermetallic compound was suggested for the as-delivered state. A phase similar to Al3Fe2Si3 can be supposed according to [15,16].

In general, XRD investigations delivered no clarity about additional intermetallic compounds due to complexity of the alloy S263.

## 4. Conclusions

By spray-compacting, material combinations not producible by the conventional melting route can be manufactured. Therefore, advantageous properties including increased wear resistance and mechanical properties can be realized. Due to the production route, a consolidation step to densify remaining pores is necessary to improve crack-propagation behavior. Extruding is usually used, thereby resulting in round stock and ensuring a constant natural strain of the spray-compacted cone. It also restricts available semi-finished products of spray-compacted alloys.

By laser welding, reasonable microstructures for all investigated hypereutectic Al-Si-alloys could be obtained for a wide range of welding speeds, implying reasonable production costs. Despite the large temperature range of solidification, no hot cracks were observed. The formation of equally distributed small precipitations annihilates thermal contraction strains on a microscopic scale. This is in opposition to conventionally casted materials.

With laser welding, an alternative joining technology to stir-friction welding, has become available. Flat semi-finished products of spray-compacted Al-Si-materials could thus be produced at high speed and reasonable cost.

**Author Contributions:** Thomas Gietzelt conceived this work, interpreted EDX measurements and morphologies, depending on different alloys, and wrote the paper (corresponding author). Torsten Wunsch conducted the sample

preparation and practical laser welding experiments. Florian Messerschmidt was responsible for preparation, metallography and SEM pictures. Uta Gerhards performed microprobe analysis and interpretation of EDX measurements. Holger Geßwein performed XRD measurements and interpretation.

**Conflicts of Interest:** The authors declare no conflict of interest.

## References

1.  Wolf, M. Zur Phänomenologie der Heißrissbildung beim Schweißen und Entwicklung aussagekräftiger Prüfverfahren. Ph.D. Thesis, University of Hamburg, Hamburg, Germany, September 2006.
2.  Uhlenwinkel, V.; Achelis, L.; Bauckhage, K. *Symposium Sprühkompaktieren*; SFB 372: Bremen, Deutschland, 2004; Volume 7, pp. 123–136.
3.  Kainer, K.U. *Metallische Verbundwerkstoffe*; Wiley-VCH: Weinheim, Germany, 2003; pp. 232–240.
4.  Rose, A. Verzugsreduzierung beim Wärmebehandeln von Bauteilen aus sprühkompaktierten und gießtechnisch hergestellten Aluminiumlegierungen durch Gasabschrecken. Ph.D. Thesis, University of Bremen, Bremen, Germany, July 2014; pp. 29–34.
5.  Roos, A. Grundlegende Untersuchung über ein neues Schweißverfahren namens HFDB. Ph.D. Thesis, GKSS-Forschungszentrum Geesthacht, Geesthacht, Germany, August 2010.
6.  Su, J.Q.; Nelson, T.W.; Sterling, C.J. Grain refinement of aluminum alloys by friction stir processing. *Philos. Mag.* **2006**, *86*, 1–24. [CrossRef]
7.  Kaufmann, S.; Fleckenstein, M. *Lasermaterialbearbeitung im Automobilbau*; Springer-VDI-Verlag GmbH: Duesseldorf, Germany, 2001; Volume 143, pp. 31–35.
8.  Sefler, P.; Wallmeroth, K.; Mann, K. *Stab, Faser und Scheibe—Die Geschichte des Festkörperlasers, Laser Magazin*; Magazin Verlag Hightech Publications KG: Bad Nenndorf, Germany, 2010; pp. 6–9.
9.  Prange, W. Maßgeschneiderte Werkstoffe für den Automobilbau. *Automob. Z.* **2001**, *2*, 140–141. [CrossRef]
10. Material Data for DISPAL-Alloys. Available online: http://www.lookpolymers.com/ (accessed on 24 June 2016).
11. Tschegg, S.E.S.; Mayer, H.; Schuller, R.; Przeorski, T.; Krug, P. Fatigue properties of spray formed hypereutectic aluminium silicon alloy DISPAL® S232 at high and very high numbers of cycles. *Mat. Sci. Eng. A Struct.* **2012**, *538*, 327–334. [CrossRef]
12. Binary Phase Diagrams, Landolt-Börnstein. Available online: http://materials.springer.com/ (accessed on 24 June 2016).
13. Bestimmung von α- und β-AlFeSi-Phasen in Aluminium-Knetlegierungen; Trimet Aluminium Ag. Available online: http://www.trimet.eu/de/fe-veroeffentlichungen/trimet_phasen_in_aluminium-knetlegierungen.pdf (accessed on 19 October 2016).
14. XRD-Online Data Base. Available online: http://cod.iutcaen.unicaen.fr/ (accessed on 26 October 2016).
15. Gueneau, C.; Servant, C.; D'Yvoire, F.; Rodier, N. $Fe_2Al_3Si_3$. *Acta Cryst.* **1995**, *51*, 2461–2464. [CrossRef]
16. Gupta, S.P. Intermetallic Compound Formation in Fe-Al-Si Ternary System: Part I. *Mater. Charact.* **2002**, *49*, 269–291. [CrossRef]